Planning of the ACS Ultradeep Field

Shardha Jogee, Harry Ferguson, Massimo Stiavelli,
Nino Panagia, and Adam Riess

Contents

List of Tables

List of Figures

1 Introduction

The Advanced Camera for Surveys (ACS) Ultra Deep field (UDF) is expected to use $\sim$ 300-400 orbits of Director's Discretionary (DD) time, most likely spread out between Cycle 11 and 12. It offers an array of potential scientific returns such as probing the tail of the reionization epoch, studying the faint end of the galaxy luminosity function, assessing surface brightness bias in the SFR history derived from the Hubble Deep Field (HDF), and studying galaxy morphology and structure with images of unprecedented depth and resolution. Several questions pertinent for the planning of the UDF merit discussion:

1. Which scientific goals should the the UDF focus on?
2. How many and which filters should be used for the UDF?
3. Should one or two fields be selected? Which one (s)?
4. What are the benefits and limitations of choosing a UDF field which lies in the continuous viewing zone (CVZ) ?
5. What are the recommended strategies for searches and followups of type Ia and type II supernovae?
6. Should a slitless grism image be included?

This draft presents material related to some of these questions, particularly items (2) (4) and (5). We refer the SAC to complementary reports which cover in more detail other issues such as field selection (report by M. Stiavelli, H. Ferguson, & N. Panagia), and grism/prism observations (report by J. Rhoads, S. Malhotra, & Z. Tsvetanov).

2 Depth of the UDF

Estimates of the potential depth of the UDF were done with a customized idl routine The depth or limiting 10 σ AB magnitude for extended sources is computed by summing the counts in a 0.2 square arcsecond square aperture, equivalent to a $0.5''$ diameter circular aperture. Updated zero point AB magnitudes from the STSDAS synphot package are used and adopted parameters include 2 readouts (i.e. 1 CR-split or a 2-point dither) per orbit, a WFC detector dark current of 2.2 x 10^{-3} electrons s^{-1} pix^{-1}, a readnoise of 5 electrons and a default gain of 1. The impact of different sky background levels were considered. At $\lambda > 3000$ Å, Earthshine (scattered Earth light) and Zodiacal light tend to dominate the sky background while airglow lines and geocoronal lines are important in the ultraviolet. Results were cross-checked with ETC for consistency.

Figure 1 shows the WFC depth for extended sources as a function of on-source exposure time, assuming dark sky conditions (equivalent to Zodiac=Low, Earthsine=low

in ETC). Table 1 and Fig. 4 show some of values and comparisons with other *HST* surveys such as the ACS Great Observatories Origins Deep Survey (GOODS; Giavalisco et al. 2001), and the WFPC2 HDF (Williams et al. 1996). Note the following points :

- For a 4-band imaging strategy with $\sim$ 100 orbits per optical broadband filter (such as F435W, F606W, F775W), the UDF reaches $\sim$ *1.3 mag deeper than the HDF (Table 1).* The gain of 3.3 in flux is coupled with the factor of 1.8 increase in field of view ($202'' \times 202''$ vs. $150'' \times 150''$) and 2 in angular resolution ($0.05''$ vs. $0.1''$), leading to a *six-fold increase* in effective surveying power in the optical regime (Figs. 1 and 3). The corresponding depth increase *w.r.t GOODS is* $\sim$ *2 mag.*

- In going from 100 to 200 orbits per WFC broadband filter, the gain in depth is $\sim$ 0.4 mag. This would be the tradeoff between a 2-bands versus a 3-bands or 4-bands optical imaging strategy (Fig. 1 and Table 1).

- If the UDF field is chosen to lie in the CVZ, UV observations or narrowband optical observations during the daytime part of 400 CVZ orbits can be obtained for free (i.e. without significant loss of the darktime for broadband optical imaging). In particular, WFC/F892N observations (§ 4, option I) can probe $\sim$ 6.3 Lyα emitters with a limiting flux below the unlensed flux of the highest redshift galaxy reported to date (Hu et al. 2002). The large ACS/WFC field of view offers the potential of detecting several tens of such sources.

3 Filter Selection

The choice of filters is guided by (i) the targeted science, (ii) a tradeoff between depth and color information, and (iii) optimal use of unique ACS capabilities not provided by WFPC2 or the upcoming WFC3 in 2005. It is beyond the scope of this draft to discuss all possible filter combinations, but we summarize here some factors to consider and the most promising options.

- Ideally an ACS UDF would make use of the F850LP filter which is a unique ACS capability. It offers a larger wavelength resolution in the red than WFPC2 broad filters such as F814W. When used with two adjacent filters, F850LP enables high redshifts systems close to the epoch of reionization ($\sim$ 7) to be separated out using the Lyman break technique. For instance, in the (F606W, F775W, F850LP) color-color plane (Fig. 9), $z \sim 4--6$ targets can be selected as F606W dropouts (e.g., F606W-F775W > 1.4) and $z \sim 6--8$ targets as F775W dropouts (e.g., F775W-F850LP > 3), with possible significant contamination from lower redshift systems.

- With the expected depth of the UDF, ground-based follow ups to get colors/redshifts of targets are not viable. Therefore, the required color information has to come from the ACS observations themselves. Color information from only

2 bands has a small dynamic range: at least 3 bands are needed for the Lyman break technique and 4 filters give robust photometric redshifts enabling objects at intermediate and high redshifts to be selected. Below are possible 3-band and 4-band filter combinations.

- **(F435W+F606W+F775W+F850LP) combination :** The WFC/F606W filter is the most sensitive for optical imaging and significantly more sensitive (by $\sim$ 0.5 mag) than F555W, the Sloan Digitized Sky Survey (SDSS) r filter (Fig. 1). Given that color identification of objects (dropouts) works best with *four adjacent filters with little overlap,* a multi-band imaging program using F606W should exclude F475W (SDSS g)and F555W (SDSS r) as they overlap significantly with F606W. Instead, F435W on the blue side of F606W and either (F775W+F850LP) or F814W on the red side could be selected. The use of F775W+F850LP rather than F814W gives extra wavelength resolution allowing redshifts close to the epoch of reionization to be separated out. This leads us to a choice of (F435W+F606W+F775W+F850LP), which is also used by the GOODS program. With this filter set galaxies at z= 2–4, z=4–6.1, and potentially z=6–8 can be selected, respectively as F435W, F606W, and F775W dropouts (see Fig. 9).

- **(F606W+F775W+F850LP) combination:** This filter selection is suitable for identifying $z \sim 6$ objects close to the tail of the reionization epoch, via the Lyman Break technique, making optimal use of F850LP (see Fig. 9). In the (F606W, F775W, F850LP) color-color plane (Fig. 9), $z \sim 4 - -6$ targets can be selected as F606W dropouts (e.g., F606W-F775W > 1.4) and $z \sim 6 - -8$ targets as F775W dropouts (e.g., F775W-F850LP > 3), with possible significant contamination from lower redshift systems. The (F606W+F775W+F850LP) combination does not enable reliable color identification of lower redshift ($z < 3$) objects in the HDF to address surface brightness bias issue in the SF history at $z \sim$ 1–3 derived from HDF. due to the loss of wavelength resolution in the red.

- **(F475W+ F555W+F775W+F850LP) combination :** This combination corresponds to the SDSS g, r, i, z set. Similar considerations apply as above. We are more sensitive by $\sim$ 0.2 mag in the blue with F475W, but lose sensitivity in the red by by giving up F606W.

- **For CVZ targets :(any of the above in darktime) + (WFC/narrowband filter or WFC/UV broadband filter or SBC/F150LP in bright time):** If the UDF targets a CVZ field, then WFC/narrowband optical observations or SBC/UV or WFC/UV broadband observations could be taken 'for free' during the daytime part of the orbit, with little loss of the darktime available for broadband optical imaging at night. The best alternative for daytime observations seems to be WFC/F892N (§ 4).

  For further information or clarification: please contact Shardha Jogee, Harry Ferguson, & Massimo Stiavelli.

4 CVZ targets: UV and narrowband observations

Most targets are occulted in part of every HST orbit except for targets which lie in the continuous viewing zone. CVZ targets can be observed without occultation for a fraction of time during the 56 day HST precessional cycle. Depending on the telescope position and the target, there may be up to 7 CVZ intervals with durations ranging between 1 to 105 orbits. *Observing efficiency of targets in the CVZ is about twice that of non-CVZ observations.* For instance, a non-CVZ target has a visibility time (amount of unocculted time per orbit) typically ranging from 44 m to 55 m. For CVZ targets the corresponding visibility time is the entire orbital time of 96 m. A significant fraction of this time (typically 30 to 40% or 28 to 40m) has a large optical sky background produced mostly by Earthshine, particularly during the daytime part of the CVZ observations. Earthshine is a strong function of the angle A_e of the observations with respect to the Earth bright limb. For instance, Earthshine can vary from V=18.0 to 23.4 mag arcsecs^{-2} as A_e changes from 16 to 52 °. The bright sky background strongly impacts broadband optical imaging, but can have minimal effect on narrowband optical imaging and select ultraviolet observations as shown in Fig. 3. *The advantage of CVZ fields is that the bright time can be optimally used for low background observations namely, select UV observations or optical narrowband observations, with only minimal loss in the available dark time for broadband optical observations.* This advantage was one of the prime factors for the selection of the HDF-N field to be in the CVZ.

We have explored three types of observations (I, II, III below) that can be carried out in CVZ bright time. Option I seem to be the most promising as it covers the entire WFC fov in one pointing and provides limiting fluxes probing an interesting redshift regime. Options II and III both cover a small fraction (3% to 36 %) of the entire WFC fov and require a tradeoff between coverage and depth.

I. WFC/narrowband optical imaging WFC/narrowband optical imaging offers the option of probing Lyα emitters from redshifts z $\sim$ 3.1 out to z $\sim$ 6.3, close to the tail of the epoch of reionization as shown in Table 2. In particular , a limiting flux of 3×10^{-18} erg cm^{-2} s^{-1} for z $\sim$ 6.3 Lyα emitters by observing with WFC/F892N during the bright time of 400 CVZ orbits assuming 30 m of bright time per orbit. *This limit is a factor of $\sim$ 10 lower than the observed flux of the lensed galaxy at z $\sim$ 6.56 reported by Hu et al. (2002) and 2 times lower than its unlensed flux* . Furthermore, the volume probed for Ly-alpha emitters with a single WFC/F892N field is $\sim$ 2400 Mpc^3 which is $\sim$ 20 times larger than the region studied by Hu et al. (2002). If the galaxy observed by Hu et al. (2002) and their density estimates are representative, we expect to see several tens of such sources in a single ACS/WFC field. This is illustrated in Fig. 5. Thus, WFC/F892N observations 'for free' during bright CVZ time offer the exciting possibility of probing Lyα emitters close to the epoch of reionization. Another complementary option here is ACS ramp filter imaging down to wavelengths longer than 1 micron, offering the possibility of pushing the redshift limit even further. 2% bandpass ramp filters, and a 9% FR914M filter are being considered. We also note that if the dark time of CVZ orbits were to use the (F606W+F775W+F850LP) filter combination, this would give additional leverage in identifying $z \sim 6$ objects.

II. SBC/UV and HRC/UV imaging The ACS Solar Blind Channel (SBC) MAMA detector has a high UV quantum efficiency, high throughput, low detector dark current (1.2 x 10^{-5} electrons s^{-1} pix^{-1}), no read noise and low sky background. A large drawback, however, is that the field of view ($35'' \times 31''$) is 40 times smaller than that of WFC. Figure 2 shows the depth achieved with different SBC UV filters in bright time. The expected total bright time is 720 kilosec if we assume 30 m of bright time per 96m CVZ orbit and a total of 400 CVZ orbits. The best SBC filter is F150LP which has a large throughput and a bandpass that minimizes the airglow and geocoronal lines F150LP can also provide by far the best constraints on the escaping Lyman-continuum from galaxies at $z \sim 1$. With 400 CVZ orbits, SBC/F150LP observations of a single field, covering $\sim 3\%$ of the ACS/WFC field, reach 30.42 AB mag (Fig. 2). *This is deeper by 2.92 mag or a factor of 15 in flux compared to very deep STIS far-UV observations GO-7410 reaching $\sim$ 27.5 AB mag at 1500 Å (Gardner et al. 2000)* HDF/F300W reached 26.98 AB mag. Covering the entire ACS/WFC field with ~ 40 SBC pointings result in a depth of $\sim$ 27.7 AB mag, not providing significant depth increase w.r.t HDF/F300W. There is no net gain in considering the HRC which has a similar field of view and lower sensitivity (Fig. 2).

III. WFC/HRC-filter UV imaging Standard WFC filters are not designed to go below pivot wavelength of 4300 Åas the WFC detector quantum efficiency (DQE) falls sharply below 4000 Å, reaching values below 10^{-26} at 3000 Å. In a non-standard mode we can use the HRC UV filters HRC–F330W (covering 2950–3750 Å) with the WFC, but the unvignetted field of view is only $\sim 72'' \times 72''$ or $\sim 36\%$ of the standard WFC field of view. As illustrated in Fig. 2, this option does not promise any significant depth increase with respect to the HDF.

CVZ Fields The CVZ is within 24 °of the orbital poles such that CVZ targets lie in a narrow range of declinations centered about $\pm$ 61.5 °. CVZ fields would therefore exclude HDF-S, equatorial fields, while allowing fields near the HDF-N. The final choice of a CVZ field would be further guided by a consideration of the scientific drivers, the need to minimize optical extinction, HI column density, IR cirrus emission, the need to avoid bright clusters in order to optimize the study of faint objects and minimize bias (For potential candidate CVZ fields, see report on UDF fields by M. Stiavelli, H. Ferguson, & N. Panagia).

Scheduling Considerations for CVZ **(1)** HST can typically observe within 15.5 °of the bright Earth limb and 7.6 °of the dark Earth limb. Earthshine is a strong function of the angle between the viewing direction and the Earth bright limb and can vary significantly during one orbit of the CVZ. Therefore observations in the UV and different optical filters must be carefully scheduled on the appropriate part of the orbits where they are least impacted by the background (see Fig. 3). In the planning and scheduling of the HDF-N, the SEAM software was used to model the time-varying zodiacal light and Earthshine during a spacecraft CVZ orbit. This software is no longer available (Larry Petro; private communication), but an alternative version can be developed. **(2)** The maximum no of contiguous uninterrupted orbits which

can be scheduled in a row would be 5–6 due to *HTS's* passage through the South Atlantic Anomaly (SAA). SAA impacts large non-CVZ programs as well, so this is not a major overhead. **(3)** There is somewhat less flexibility in scheduling observations for supernovae searches, although the suggested SN Ia search strategy of 5 orbit epochs in different filter with each filter separated by 60 day intervals (§ 5) are not inconsistent with the SAA constraint and *HST* precessional cycle of 56 days controlling recurrent CVZ observations.
For further information or clarification: please contact Shardha Jogee, Harry Ferguson, & Massimo Stiavelli.

5 Searches and Followups of Type Ia Supernovae

The following factors should be considered in optimizing supernovae searches. Any multi-orbit deep integration of a high galactic latitude field in a red bandpass is ideal for searching for distant supernovae as long as the observations are properly sequenced. The ideal spacing of successive epochs of integration for collecting type Ia supernovae of cosmological significance is (1+z) × 20 days, where 20 days is the risetime of a SN Ia (Riess et al. 1999). The redshift, z, is the target redshift and should be matched to (i.e., less than) the maximum redshift to which an epoch can detect a SN Ia at peak. Calculations and experience from GOODs indicates that 1 orbit in F850LP can comfortably reach z=1.5. To reach unique redshifts, 'epochs' of the UDF should be more than 1 orbit. Choosing a target of z=2 would require 5 orbit epochs. Simultaneous epochs of bluer colors will allow determination of the type of any supernova found.

So to maximize the likelihood of finding SNe Ia at z=2 (e.g., for rates) a sequence of 5 orbit blasts with each filter separated by 60 day intervals would be ideal. Two problems immediately arise: (1) The spacing of the search epochs is a factor of 4-5 too long to follow the light curve of a SN Ia discovered (2) it would take 2-3 years to finish the UDF! An obvious compromise is just do 1 or 2 SN searches (i.e., a 60-120 day interval for the UDF) and do many shorter 5 orbit epochs in between to follow any SN discovered. An additional point to note is that a multiple epoch program with ∼ 5–7 orbits would easily allow a range of orientations good for a slitless grism program.
For further information or clarification: please contact Adam Riess

6 Searches and Rates of Type Ia and Type II Supernovae

RATIONALE - Detecting and studying photometrically high-z (say, $z > 1.5$) SNe is of fundamental importance because it allows us to study SN rates. Even without spectroscopy (obtaining detailed spectra would be VERY hard; see below) the SN characterization can be inferred from imaging alone (see figures), and the redshifts may

be measured either from the host-galaxy spectrum (actual spectroscopy or its poor-child approximation, i.e. photometry) or even from photometry of the SNe themselves.

The rates of SNIa will be able to reveal the nature of their progenitors and/or the history of star formation for moderate mass stars (3-8 $M_\odot$).

The rates of SNII will provide a *direct* measurement of the cosmic star formation rate in the redshift interval 1-2.5, i.e. just where the peak of star formation is "expected" to occur. We like to stress that the SNII rate is a direct measurement of the death of stars with masses 8-30 $M_\odot$ (for a Salpeter IMF they include 86% of the stars above 8 $M_\odot$ and 63% of the mass in massive stars), which in steady state (over time intervals less than 30 Myrs) IS the star formation rate itself. The widely used diagnostic based on the Hα flux is probing only the upper end of the IMF, which includes about 27% of the massive stars and less than 1/2 of their total mass. Note also that the amount of processed material that is injected into the ISM/IGM is increasing less than linearly with the stellar progenitor mass and, therefore, the direct SNII rate measurement is a *much better* tool to study the chemical evolution of the Universe.

OBSERVATIONAL CONSTRAINTS AND RECOMMENDED STRATEGY

Using the observed spectra of SNIa 1992 (Kirshner *et al.* 1993, ApJ 415, 589) and SNII 1998S (Lentz *et al.* 2001, ApJ 547, 406) we computed the expected spectra of SNIa and SNII at a number of redshifts (series 1: z = 1, 1.5, 2, 2.5; series 2 z = 2, 2.2, 2.4, 2.6) for different choices of the exposure time (1, 2, 4, 8, 16, 32 orbits) in four adjacent/non-overlapping ACS bands (F475W, F606W, F775W, F850LP). In all calculations we have assumed B_{max} = -19.5 and -17.5 for SNIa and SNII, respectively. The corresponding flux limits for a S/N=10 are shown in the plots (see Figures 6 and 7).

The 1 orbit exposure time corresponds to the GOODS strategy and indeed we find that one can detect SNIa up to a maximum of z=1.5 and SNII up to about z=1.7 (cf. Table 3). It is also apparent that SNe that are detected only in the z-band are likely to be SNIa, whereas SNe detected in more bands with comparable fluxes are SNII.

We estimated the expected SN rates following the calculations by Madau, Della Valle & Panagia (1998, MNRAS 297, L12) . [Note that the detection rates of the ongoing GOODS SN search are perfectly consistent with Madau et al predictions.] Table 4 reports for SNIa and SNII: the maximum detection redshift, the observing band where the highest flux is expected and the SN rate, in units of SN/year per ACS field, for exposure times 1 through 32 orbits.

In our opinion the interesting cases to consider are 8 or 16 orbits per epoch and per band because they extend the search to redshifts beyond the expected cosmic star formation peak at about z=1.5-2.

The widths of the light curves (defined as δt(1 mag)) at the appropriate wavelengths (about 2400Å and 2800Å for SNII and SNIa, respectively; see Panagia *et al.* 1980, MNRAS 192, 861, Kirshner *et al.* 1993; Figure 8) are about 15-20 days for both SNII and SNIa near their limiting detection redshifts.

It follows that if one wants to cover ALL events that occur in a given field one should make observations at time intervals no longer than 45-60 days.

A possible strategy, then, would be to observe at 8 epochs, at 1.5 mos intervals,

which corresponds to a total exposure of either 64 or 128 orbits per band.

From the point of view of maximizing the SN detections, it is apparent that (a) monitoring TWO fields at 8 epochs with exposures of 8 orbits at each epoch is MUCH MORE ADVANTAGEOUS than (b) monitoring ONE field at 8 epochs with exposures of 16 orbits. In the two field option (a) one expects to detect about 17±4 SNII and 4±2 SNIa, whereas in the one field option (b) only 10±3 SNII and 3±1.7 SNIa would be expected.

POSSIBLE ENHANCEMENTS

• Stacking the observations made at each epoch in two or more bands (most importantly the V and I bands for SNII, and the I and z bands for SNIa) will provide even deeper images that can be used to detect SNe that would fall below the detection limit otherwise.

• Adopting one of the GOODS fields (or similarly deep, multiband fields) would add the first epoch observation *"for free"*.

For further information or clarification: please contact Nino Panagia.

7 Acknowledgments

We are grateful to Ron Gilliland, Mark Clampin, Guido de Marchi, Larry Petro, and Adam Welty for discussions.

Table 1: **Comparison of UDF, GOODS, and HDF limiting magnitude**

(1) Imaging mode	(2) Pivot λ [Å]	(3) On-source Time [kilosec]	(4) No of orbits	(5) 10 σ AB mag[1]
		UDF		
WFC/F435W	4311.80	24.0	10.0	27.9286
WFC/F435W	4311.80	120.0	50.0	28.8126
WFC/F435W	4311.80	180.0	75.0	29.0342
WFC/F435W	4311.80	240.0	100.0	29.1913
WFC/F435W	4311.80	480.0	200.0	29.5693
WFC/F606W	5915.38	24.0	10.0	28.2768
WFC/F606W	5915.38	120.0	50.0	29.1569
WFC/F606W	5915.38	180.0	75.0	29.3780
WFC/F606W	5915.38	240.0	100.0	29.5348
WFC/F606W	5915.38	480.0	200.0	29.9121
WFC/F775W	7697.34	24.0	10.0	27.6346
WFC/F775W	7697.34	120.0	50.0	28.5161
WFC/F775W	7697.34	180.0	75.0	28.7374
WFC/F775W	7697.34	240.0	100.0	28.8943
WFC/F775W	7697.34	480.0	200.0	29.2719
WFC/F850LP	9103.29	24.0	10.0	27.1026
WFC/F850LP	9103.29	120.0	50.0	27.9858
WFC/F850LP	9103.29	180.0	75.0	28.2073
WFC/F850LP	9103.29	240.0	100.0	28.3643
WFC/F850LP	9103.29	480.0	200.0	28.7422
		GOODS		
WFC/F435W	4311.80	7.2	3.0	27.2000
WFC/F606W	5915.38	6.0	2.5	27.5000
WFC/F775W	7697.34	6.0	2.5	26.8000
WFC/F850LP	9103.29	12.0	5.0	26.7000
		HDF		
WFPC2/F300W	2992.00	153.7	64.0	26.9800
WFPC2/F450W	4556.47	120.6	50.0	27.8600
WFPC2/F606W	6001.06	109.0	45.0	28.2100
WFPC2/F814W	8001.61	123.6	51.0	27.6000

Notes: (1)Column 5 is the limiting 10 σ AB magnitude for extended sources assuming a 0.2 square arcsecond square in all three surveys. For the UDF, we assume an exposure time of 240 kilo seconds ($\sim$ 100 orbits), 1 CR-split or a 2-point dither per orbit, and low sky background (Zodiac=Low, Earthshine=Ave)in the optical.

Table 2: **WFC/narrowband imaging during bright CVZ time**

(1) Imaging mode	(2) On-source time [kilosec]	(3) z(Lyα)	(4) Emission flux[1] erg cm^{-2} s^{-1}
WFC/F502N	20.0	3.13	2.8e-17
WFC/F502N	100.0	3.13	1.2e-17
WFC/F502N	200.0	3.13	8.4e-18
WFC/F502N	800.0	3.13	4.2e-18
WFC/F658N	20.0	4.41	1.3e-17
WFC/F658N	100.0	4.41	5.6e-18
WFC/F658N	200.0	4.41	4.0e-18
WFC/F658N	800.0	4.41	2.0e-18
WFC/F660N	20.0	4.43	1.7e-17
WFC/F660N	100.0	4.43	7.4e-18
WFC/F660N	200.0	4.43	5.2e-18
WFC/F660N	800.0	4.43	2.6e-18
WFC/F892N	20.0	6.34	2.0e-17
WFC/F892N	100.0	6.34	8.7e-18
WFC/F892N	200.0	6.34	6.1e-18
WFC/F892N	800.0	6.34	3.0e-18

Notes: (1) Column 4 is the limiting 10 σ flux for an extended Ly α-emitting source at a redshift z(Lyα), assuming a 0.2 square arcsecond square aperture.

Table 3: **Limiting redshifts, bands of max. flux, expected SNIa & SNII rates**

	SNIa			SNII		
Exp. Time	z_{max}	band(F_{max})	SN/yr	z_{max}	band(F_{max})	SN/yr
1 orbit	1.5	z-band	1.2	1.5	V-band	3.2
2 orbits	1.6	z-band	1.4	1.8	V-band	5.7
4 orbits	1.7	z-band	1.6	2.0	I-band	6.7
8 orbits	1.8	z-band	1.8	2.2	I-band	8.5
16 orbits	2.0	z-band	2.4	2.5	I-band	10.4
32 orbits	2.1	z-band	2.7	2.7	I-band	11.0

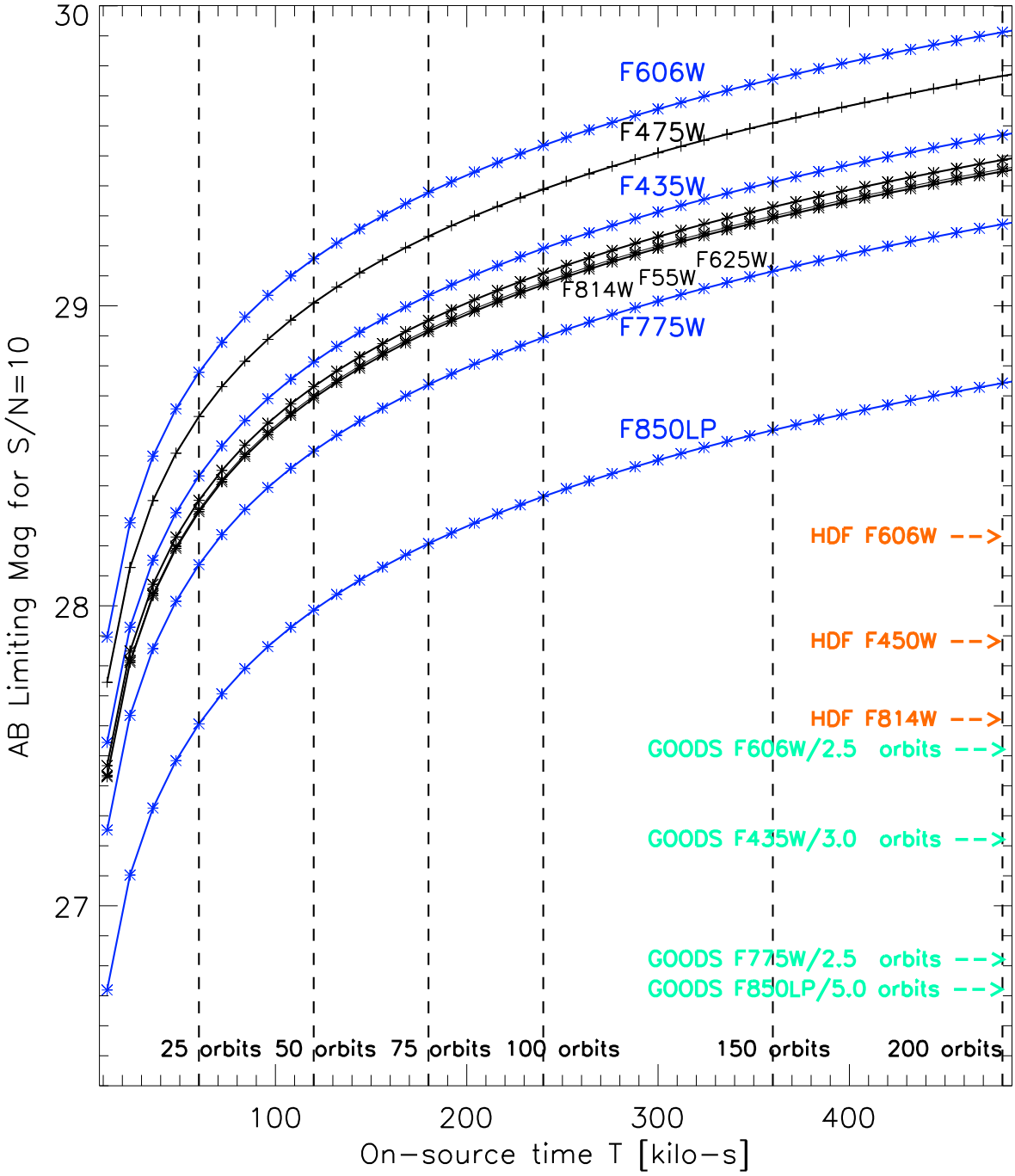

Figure 1: **UDF Depth and Exposure Time Tradeoff (WFC):** The limiting 10 σ AB magnitude for extended sources assuming a 0.2 square arcsecond square aperture is plotted as a function of on-source exposure time T for WFC/broadband optical imaging. Dark sky conditions (equivalent to Zodiac=Low, Earthshine=Ave in ETC) and 2 readouts (i.e. 1 CR-split or a 2-point dither) per orbit are assumed. The vertical dashed lines indicate the number of orbits corresponding to T, assuming 2400 s of on-source dark time per orbit.

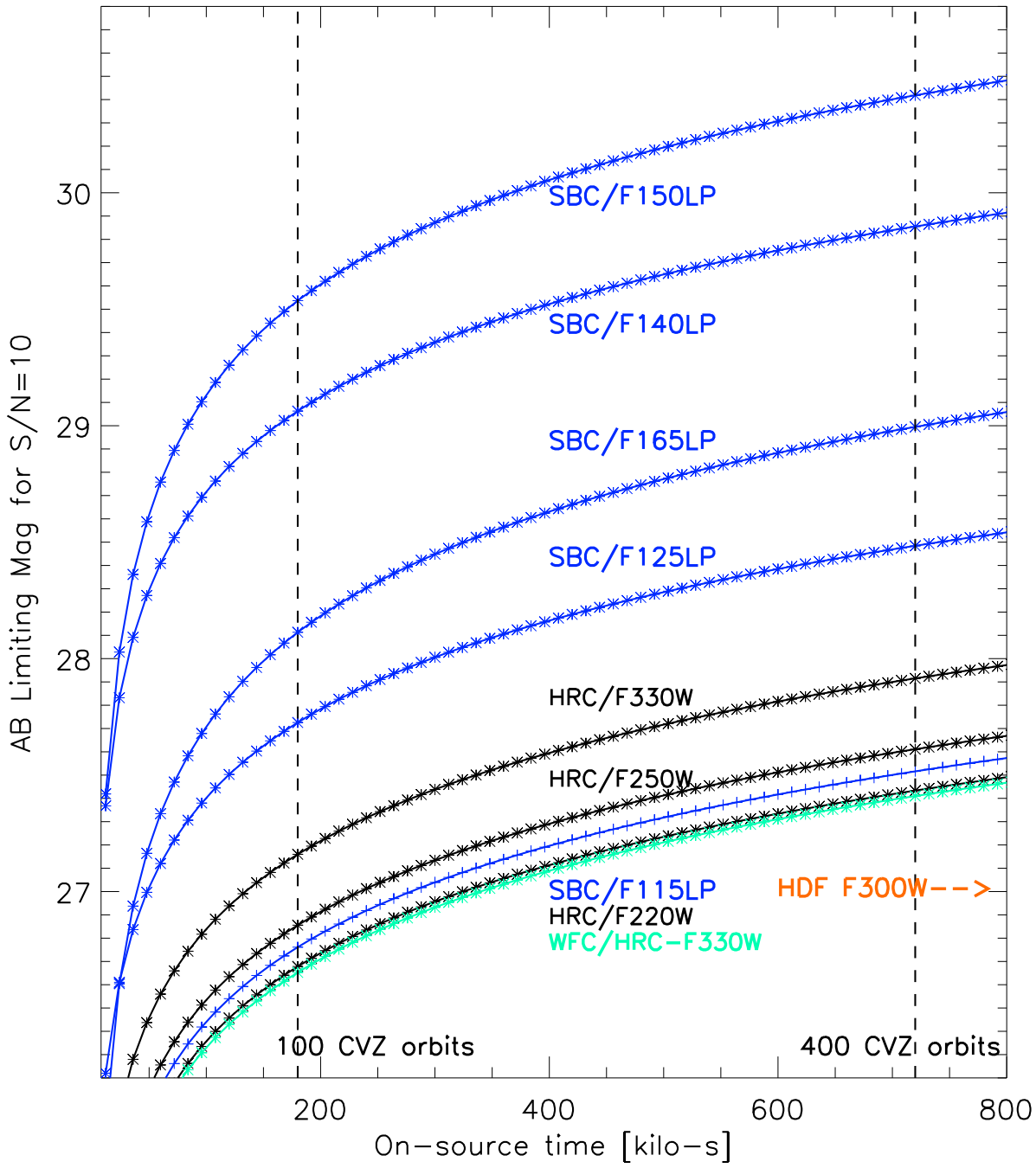

Figure 2: **SBC/UV, HRC/UV, WFC/HRC-UV observations in bright CVZ time:** Plotted are the limiting 10 σ AB magnitude for extended sources observed in bright CVZ time (equivalent to Zodiac=High, Earthshine=High in ETC). 720 kilosec of bright time is available assuming 30 m of bright time per orbit for a total of 400 CVZ orbits. Note that WFC/HRC-UV setups use HRC filters with the WFC and cover $\sim$ 30 % of the standard WFC fov. SBC/UV and HRC/UV cover 3% and 5% of the standard WFC fov. For reference, the limiting magnitude of the HDF is marked.

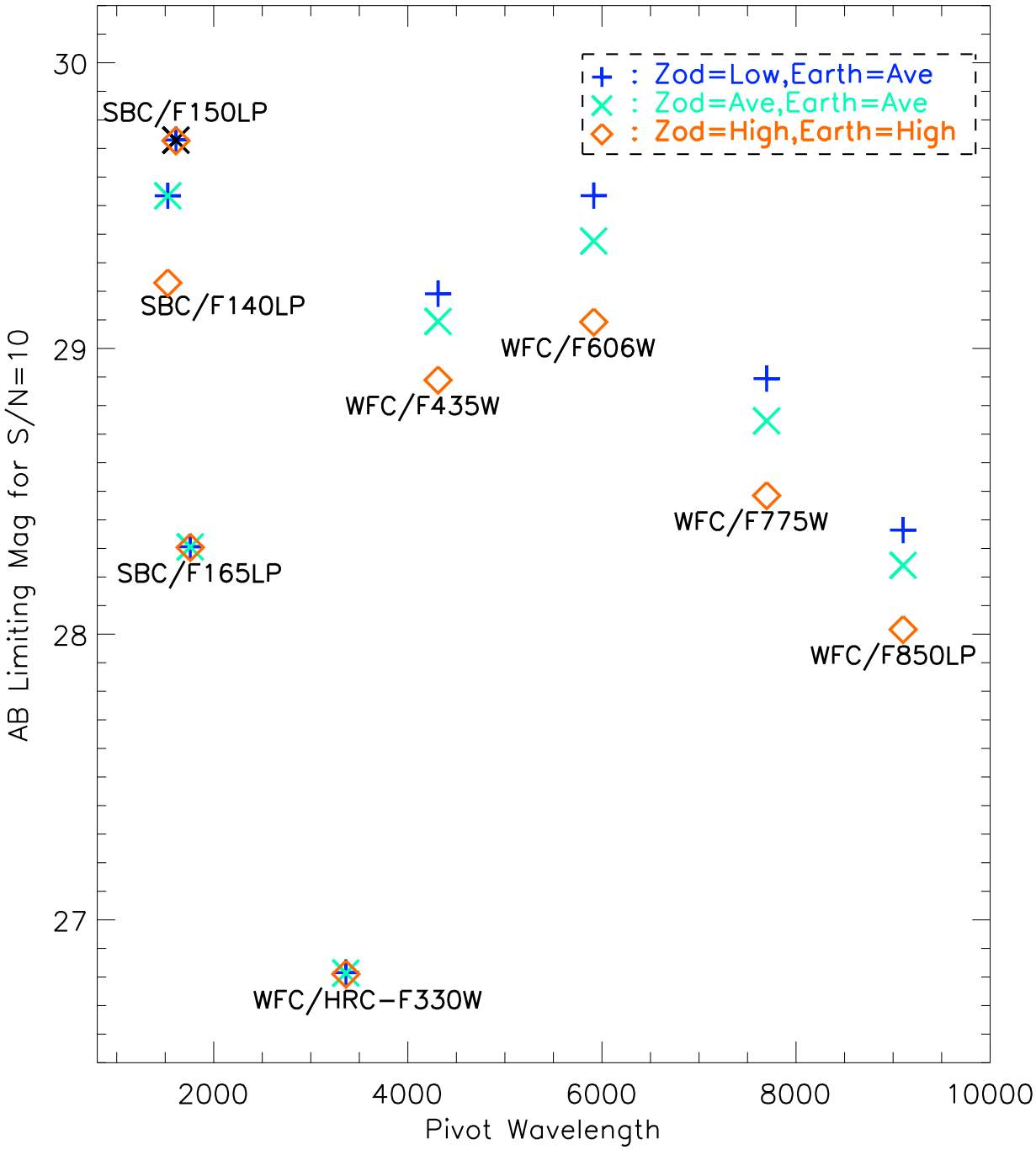

Figure 3: **Effect of Sky Background on SBC and WFC Depths:** Plotted are the limiting 10 σ AB magnitude for extended sources observed with the SBC/UV, WFC/HRC-F330W, and WFC/broadband optical filters under low, average and bright sky conditions. An on-source exposure time of 240 kilosec is assumed. Note that the limiting depths of the SBC/F150LP, SBC/F165LP, and WFC/HRC-F330W configurations are nearly independent of the sky background.

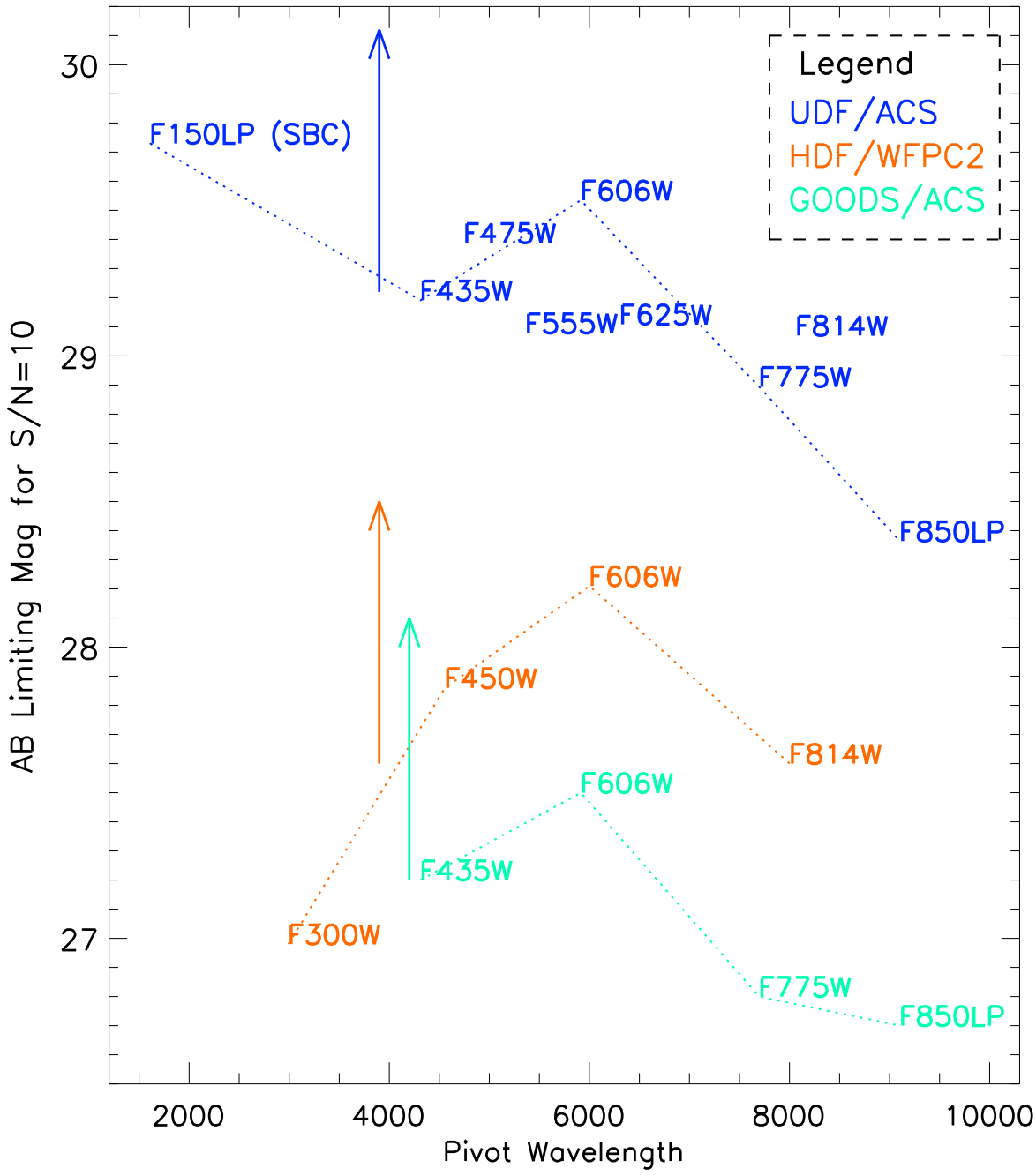

Figure 4: **Limiting Magnitude of HST Imaging Surveys:** Plotted are the limiting 10 σ AB magnitude for extended sources in different *HST* surveys, assuming a 0.2 square arcsec aperture. For the UDF, plotted values assume an exposure time of 240 kilosec ($\sim$ 100 orbits), 1 CR-split or a 2-point dither per orbit, low sky background in the optical and high sky background in the UV. For point sources, the limiting magnitude is $\sim$ 0.8 mag fainter as shown by the arrows. Note that the SBC covers only 3% of the WFC field of view.

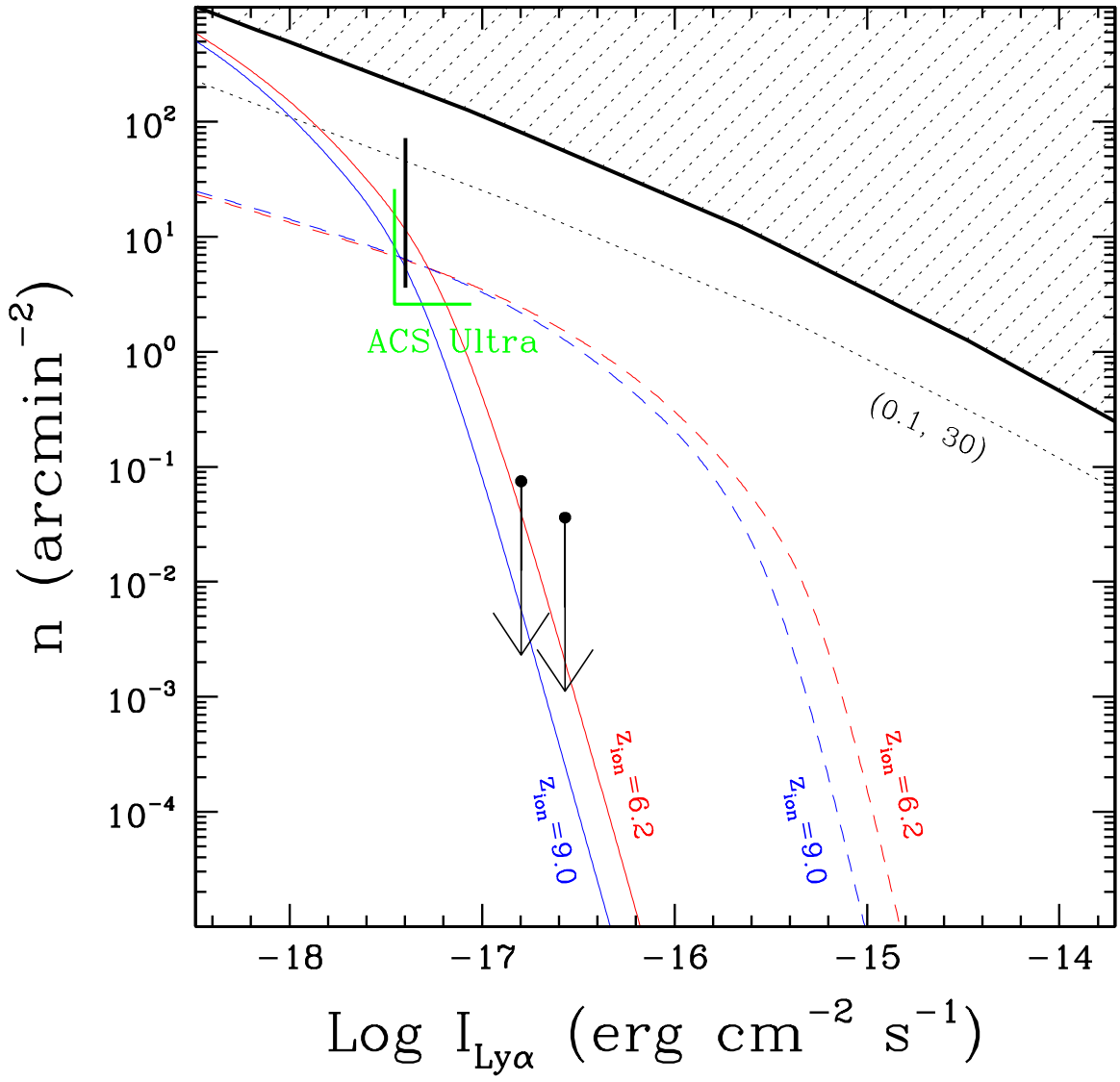

Figure 5: **Surface density vs Lyman α line flux of reionization sources:** The solid bar represents the density estimated from the detection at $z = 6.56$ by Hu et al. (2002) while the two points with down-pointing arrows represent their upper limits. The thin dotted line indicates the locus of identical sources for $z_{reion} < 10$. The (0.1, 30) model combines a 10 % escape of Lyman continuum photons with a standard value for the clumpiness of neutral hydrogen (after Stiavelli et al. 2002, ApJ submitted). The dashed lines show the cumulative Lyman α luminosity function of reionization sources for the (0.1, 30) model and $M_\star$ -17.5. As an illustration, we also show as solid lines show the cumulative Lyman α luminosity function for a model with $M_\star = -10$ rescaled to pass through the Hu et al. data point. The upper and lower line in each pair are for for $z_{reion} = 6.2$ and 9, respectively. The shaded area represents models that would imply a mean metallicity of the Universe at reionization higher than 0.01 $Z_\odot$. The thick corner marker identifies identifies the area probed by a narrow band excess survey with ACS+F892N at $z = 6.33$.

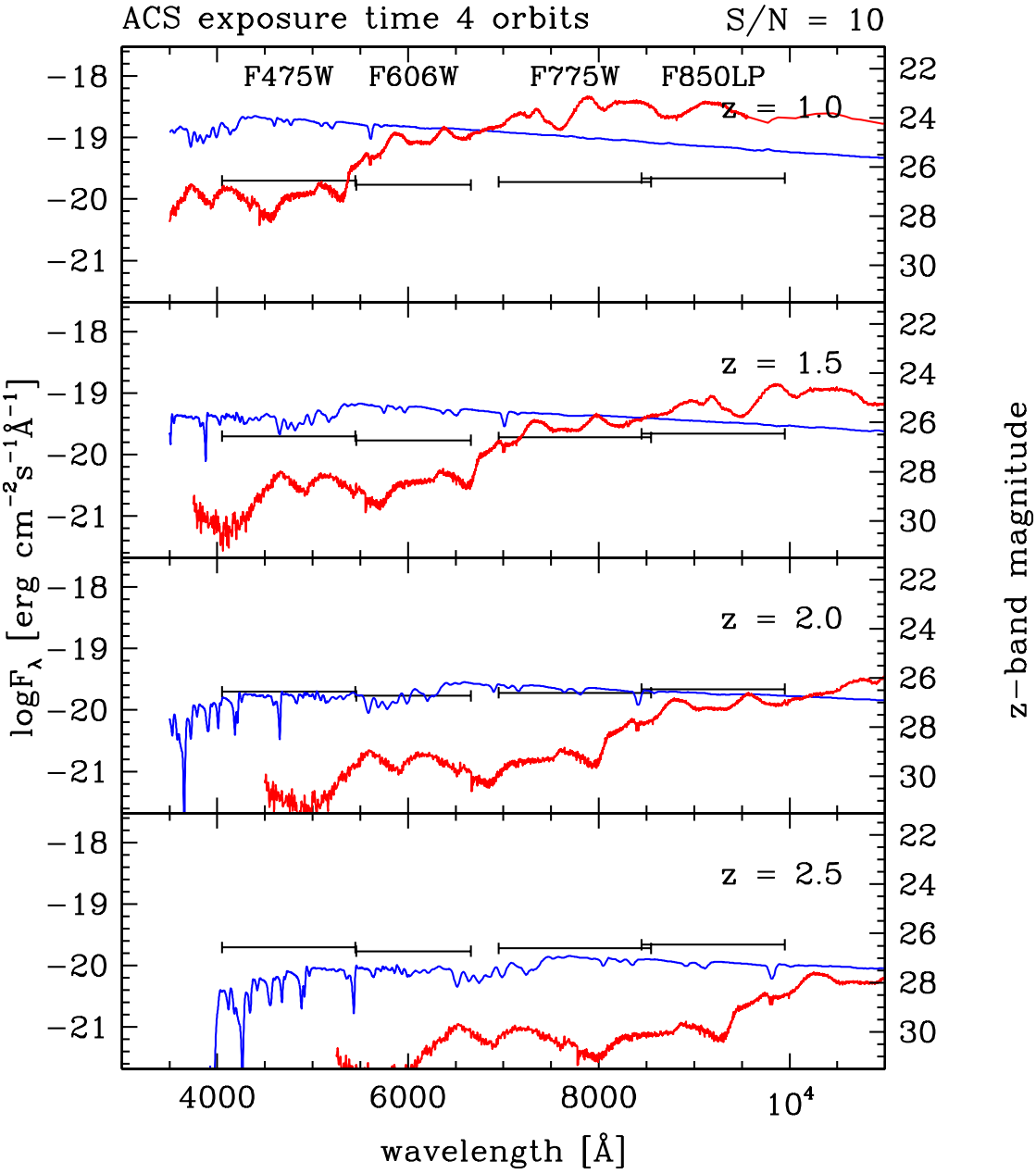

Figure 6: **Redshifted spectra of SNIa and SNII and 4-orbit limiting fluxes:** The redshifted spectra of SNIa 1992A (red curve) and SNII 1998S (blue curve) are compared with the limiting fluxes for an exposure time of 4 orbits.

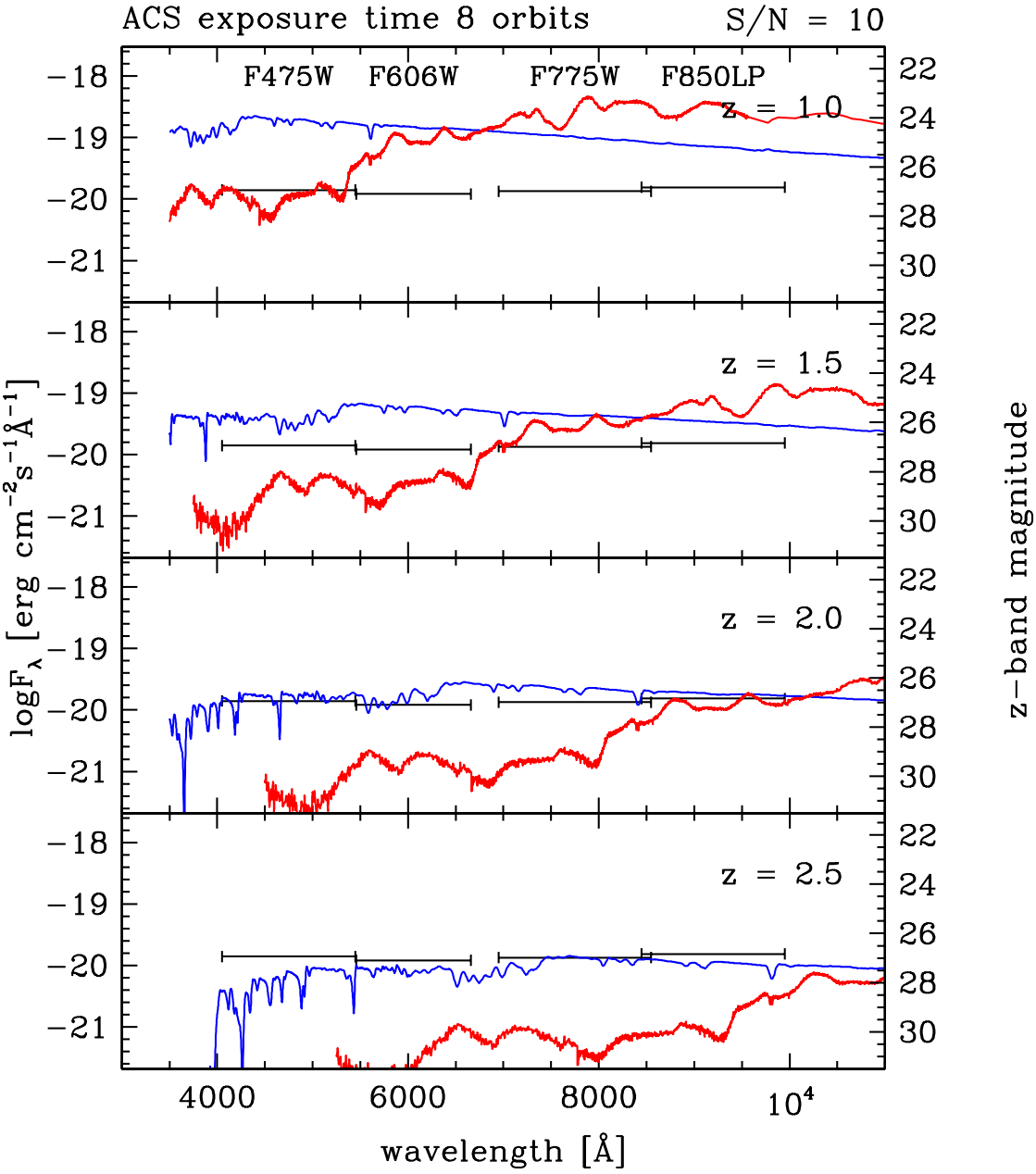

Figure 7: **Redshifted spectra of SNIa and SNII and 8-orbit limiting fluxes:** The redshifted spectra of SNIa 1992A (red curve) and SNII 1998S (blue curve) are compared with the limiting fluxes for an exposure time of 8 orbits.

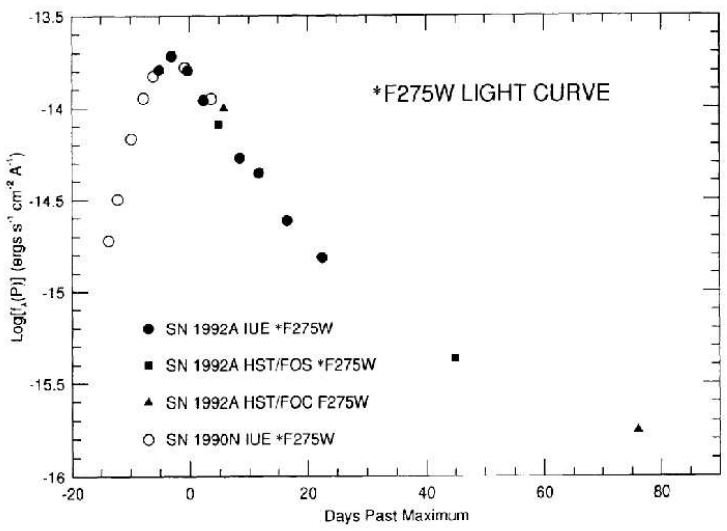

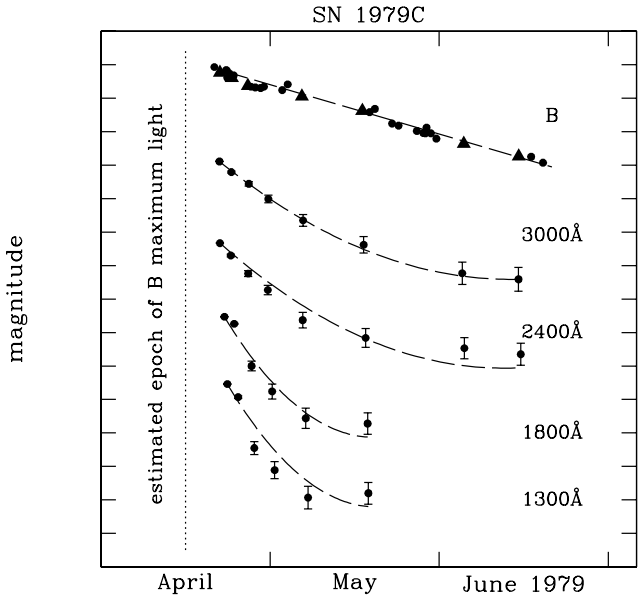

Figure 8: **UV Light curves of SNIa 1992A (top) and SNII 1979C (bottom)** (adapted from Kirshner *et al.* 1993, and Panagia *et al.* 1980).

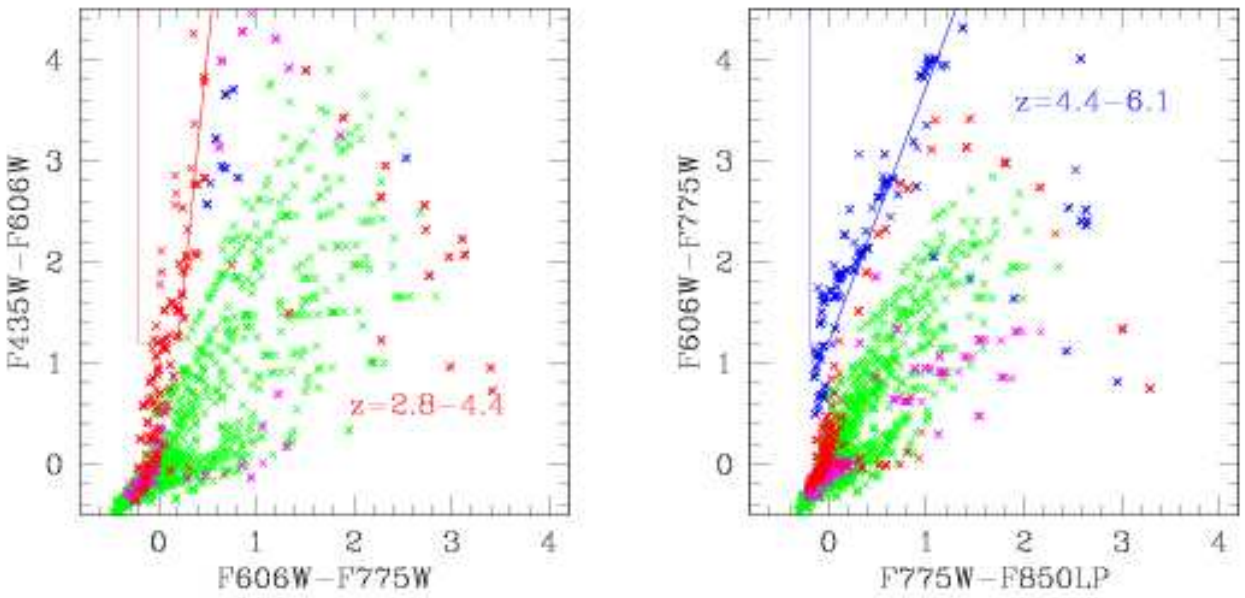

Figure 9: **Color selection:** The color-color plots show the properties of galaxy models at redshift between 0 and 10. The models include various ages, metallicities, star formation histories, and dust content. An average correction for the combined effect of the Lyman alpha forest has been also applied following Madau. Symbols of different colors correspond to different redshifts. The red contour in the left diagram identifies a possible color selection for F435W-dropout objects at z=2.8–4.4. The blue contour in the right diagram identifies a possible color selection for F606W-dropout objects at z=4.4—6.1.